Asian Journal of Chemistry; Vol. 37, No. 2 (2025), 392-400

ASIAN JOURNAL OF CHEMISTRY

https://doi.org/10.14233/ajchem.2025.33109

Enhanced Antimicrobial Activity of PVP-ALG/ZnO Nanocomposite Films with Controlled Drug Release and UV Blocking Properties

SUHAILA THATTARIL[1,2], NASHEETHA RAHMAN THYTHOTTATHIL[1] and KAVITHA MANNILEDAM[1,*]

[1]Post Graduate and Research Department of Chemistry, Zamorins Guruvayurappan College (Affiliated to University of Calicut), Kozhikode-673014, India
[2]Department of Chemistry, Government College, Kodanchery-673580, India

*Corresponding author: E-mail: kavitham@zgcollege.ac.in

Received: 30 November 2024; *Accepted*: 13 January 2025; *Published online*: 31 January 2025; AJC-21891

A novel PVP-ALG/ZnO hydrogel nanocomposite film was synthesized using a solution casting method. By incorporating ZnO nanoparticles into a polyvinylpyrrolidone (PVP) and sodium alginate (ALG) hydrogel, the nanocomposite film demonstrated enhanced antimicrobial, mechanical and UV-blocking properties. Characterization techniques, including XRD, SEM, TEM and UTM, revealed an optimal tensile strength at a 0.0075 g ZnO composition. The composite exhibited superior swelling behaviour compared to pure PVP-ALG hydrogel in distilled water and buffer solution of pH 6.8. Drug-loading studies with cephalexin showed slower, sustained release under intestinal pH (6.8), attributed to ZnO-induced interactions. Antimicrobial analysis confirmed enhanced effectiveness and UV-blocking tests highlighted a high sun protection factor (SPF) of 7.9 for the nanocomposite film. The results highlighted the potential of the PVP-ALG/ZnO hydrogel as an excellent option for use in biomedical and pharmaceutical fields, especially for sustained drug delivery and protective applications.

Keywords: PVP-ALG/ZnO nanocomposite, Swelling study, Antimicrobial, Drug delivery, UV blocking ability.

INTRODUCTION

Hydrogels, often referred to as water-containing gels, are materials composed of polymers that feature a crosslinked structure, allowing them to maintain a distinct three-dimensional configuration. They exhibit both water-attracting properties (hydrophilicity) and resistance to dissolve in water [1,2]. Due to their distinctive physical characteristics, these networks can be moulded into a variety of sizes and shapes. They possess excellent biocompatibility, ease of fabrication, diverse composition options and favourable physical properties resembling physiological conditions. Hydrogels, either alone or in conjunction with cells, find numerous applications in the field of biomedicine [3]. Hydrogels can function as support structures in tissue engineering [4], carriers for delivering drugs or genes [5], adhesives or barriers separating tissue and material [6] surfaces and cell sheets enabling reversible control of cell attachment. Although hydrogels provide numerous advantages, they also present certain disadvantages. The insufficient tensile strength of numerous hydrogels limits their use in conditions necessitating load-bearing capabilities [7], potentially resulting in early dissolution or displacement from the designated site. The amount and uniformity of drug incorporation into hydrogels might be constrained, especially when dealing with hydrophobic drugs [8]. The substantial water content and considerable pore sizes in most hydrogels frequently lead to a relatively rapid release of drugs, occurring within a span of a few hours to several days [9]. Furthermore, challenges in application arises due to the lack of injectability in certain hydrogels, the necessitating surgical implantation as a requirement for many cases. Nanoparticles have been strategically integrated into hydrogels to overcome inherent limitations, imparting unique chemical and physical characteristics to these materials. This amalgamation improves their thermal, mechanical and optical attributes, opening up a new pathway for enhanced performance [6,10].

Polyvinylpyrrolidone (PVP) is a synthetic polymer known for its biocompatibility, having served for an extensive period as a biomaterial or additive in pharmaceutical formulations [11]. Subjected to various stimuli such as radiation, heat, pressure

and chemicals, polyvinylpyrrolidone (PVP) undergoes cross-linking, resulting in the formation of PVP hydrogel. Numerous research studies have explored into the synthesis and characterization of polyvinylpyrrolidone (PVP) hydrogels [12,13]. But it has been observed that the limited adoption of PVP hydrogels is attributed to their inadequate mechanical properties and insufficient swelling capacity [14-16]. There are many detailed records exist regarding the combination of PVP and polysaccharides [11,14,17,18] to form hydrogels, as their combination is known to enhance the overall properties of the hydrogels.

Alginate is a naturally derived anionic biopolymer obtained from brown seaweed [19] and has been widely employed in various biomedical applications owing to its biocompatibility, minimal toxicity and cost-effectiveness [20]. Alginate facilitates the gel formation and generate a moist healing environment that supports re-epithelialization [21]. The synergistic use of alginate and synthetic polymers can confer the ideal properties required for effective wound repair [22]. The ability to prevent microbial infections is a crucial and highly beneficial characteristic for burn bandages and wound dressings [23,24].

Sunlight serves as a significant source of ultraviolet (UV) radiation, which can adversely affect both the skin and immune system with prolonged exposure [25,26]. To mitigate these effects, a diverse array of UV-protective materials, including sunscreens, coatings and films have been developed [27,28]. Zinc oxide (ZnO) nanoparticles are widely incorporated into sunscreens due to their capacity to effectively absorb UV radiation over a broad wavelength range [29]. Interestingly, ZnO exhibits UV protection across both macro and nanoscale forms, covering the UV-B (290-320 nm) and UV-A (320-400 nm) spectra [30]. ZnO is also recognized for its biocompatibility, biosafety and exceptional chemical and biological properties, making it an ideal candidate for UV protection applications [30,31]. The integration of ZnO nanoparticles with polyvinylpyrrolidone-alginate (PVP-ALG) hydrogels represents an innovative strategy to enhance the sunscreen performance. The polymeric cross-linked structure of PVP-ALG hydrogels facilitates the encapsulation of nanoparticles, potentially reducing skin irritation or sensitivity often associated with direct nanoparticle exposure. The current investigation concentrated on developing a hydrogel nanocomposite using polyvinyl pyrrolidone (PVP) along with alginate and integrating ZnO nanoparticles into the hydrogel network by solution casting method to explore its potential application in biomedicine and pharmaceutical field.

EXPERIMENTAL

Zinc oxide (ZnO) nanoparticles were synthesized through the coprecpitation method. A distinctive hydrogel formulation consisting of PVP, alginate, PEG, agar and glycerine was developed through solution casting approach. The hydrogel was subjected to characterization using standard methods. In the resulting hydrogel, PVP and alginate serve as base polymers, PEG functions as a healing agent, agar acts as a gelling agent [32] and glycerin plays the role of a humectant [14].

PVP K 30 (PVP: molecular weight 40,000) obtained from TCI, PEG 2000 from Merck, sodium alginate purchased from High media and agar, glycerine. NaOH and $Zn(NO_3)_2{\cdot}6H_2O$ were supplied by NICE chemicals.

Synthesis of ZnO nanoparticles: Prepared 100 mL solutions of $Zn(NO_3)_2{\cdot}6H_2O$ and NaOH separately at respective concentrations of 0.5 M and 1.0 M. Then, NaOH solution was added dropwise into the $Zn(NO_3)_2{\cdot}6H_2O$ solution with intense agitation, results in the formation of ZnO as white precipitate. The precipitate was repeatedly rinsed with distilled water and ethanol. The resulting ZnO powder underwent drying in a hot air oven at 70 ºC for 6 h, followed by annealing in a muffle furnace at 400 ºC for 2 h to improve the crystallinity [33].

Preparation of PVP-ALG/ZnO nanocomposite: For the synthesis of nanocomposite, the initial step involved crafting a hydrogel film. Hydrogel films were prepared through a solution casting method utilizing an aqueous solution containing PVP, alginate, PEG, agar and glycerine. The proportion of PVP to alginate was altered across different ratios (10:90, 20:80, 50:50, 80:20 and 90:10), while maintaining a constant concentration of other reagents. The composition of each component in the hydrogels are given in Table-1. ZnO nanoparticle was then added to the selected hydrogel having high tensile strength in various amounts (weight in grams) during the preparation of the composite film. The amount of ZnO nanoparticle in the hydrogel composite are shown in Table-2. The specified components were introduced into separate glass bottles, sealed and subjected to an autoclave at 15 lbs (107 kPa) pressure and 120 ºC for 20 min. Subsequently, the heated solution was poured into individual Petri dishes and left to cool.

TABLE-1
COMPOSITION OF PVP-ALG HYDROGEL (%)

Sample index	PVP	ALG	AGAR	PEG	Glycerin	Water
PVP-ALG (10:90)	0.1	0.9	0.2	1.0	1.0	95
PVP-ALG (20:80)	0.2	0.8	0.2	1.0	1.0	95
PVP-ALG (50:50)	0.5	0.5	0.2	1.0	1.0	95
PVP-ALG (80:20)	0.8	0.2	0.2	1.0	1.0	95
PVP-ALG (90:10)	0.9	0.1	0.2	1.0	1.0	95

TABLE-2
WEIGHT OF ZnO NANOPARTICLE IN PVP-ALG HYDROGEL (g)

Sample index	A0	A1	A2	A3	A4	A5
ZnO	0	0.0075	0.01	0.0125	0.015	0.0175

Characterization: The crystal structure was analyzed using Aeris research benchtop X-ray diffractometer and the patterns were recorded with Cu*K*α radiation (λ = 1.54060 Å). Morphology analysis was carried out using Jeol 6390LA/Oxford XMX N scanning electron microscopy (SEM), Zeiss Sigma 300 field emission scanning electron microscopy (FESEM) and Talos F200 S transmission electron microscopy (TEM). The Fourier transform infrared (FTIR) spectra of PVP-ALG hydrogel and powdered ALG and PVP were obtained using a Perkin-Elmer FTIR spectrometer, covering the range from 4000 to 500 cm^{-1}.

Measurement of mechanical properties: The tensile properties were tested in Shimadzu (AG-Xplux 10Kn) UTM. All the films were cut in the dimension of 60 mm × 10 mm and the cross-head speed was maintained at 20 mm/min. The average thickness of the film was 0.0045 mm and all the data represent a mean of three replications.

Swelling behaviour: Approximately 0.1 g of dried sample was immersed in either 50 mL of distilled water or buffer solutions (pH 1.2 and 6.8) at room temperature for 24 h. The swollen gel was extracted from the swelling medium at designated time intervals, superficially dried with filter paper, weighed and then returned to the same bath [29,30]. Percentage swelling (Ps) of hydrogel was calculated using the following formula:

$$\text{Swelling } (\%) = \frac{W_s - W_d}{W_d} \times 100$$

W_s = weight of dried sample, W_d = weight of swollen sample.

Drug loading: In this study, cephalexin was selected as the model drug for encapsulation. The drug-loading process was conducted by immersing 0.2 g of each sample into a 50 mL cephalexin solution prepared in distilled water, maintained at 37 ºC, for 48 h. Following the encapsulation period, the drug-loaded hydrogels were extracted, thoroughly washed and subsequently dried. The drug loading efficiency was evaluated using the following equation [34]:

$$\text{Drug loading capacity} = \frac{\text{Weight of drug in the substrate}}{\text{Weight of the substrate}} \times 100$$

***In vitro* drug release studies:** The release profile of cephalexin from the hydrogels was studied in a medium with a pH of 6.8, mimicking the intestinal fluid environment. For this purpose, 0.2 g of drug-loaded hydrogels was immersed in 50 mL of the release medium at 37 ºC under constant magnetic stirring at a speed of 50 revolutions per min. At predetermined intervals, 5 mL aliquots of the solution were withdrawn and the concentration of cephalexin released was quantified using a UV spectrophotometer at a wavelength of 262 nm. The amount of drug released was then calculated using the following formula [35]:

$$\text{Drug release } (\%) = \frac{\text{Amount of released drug}}{\text{Amount of loaded drug}} \times 100$$

Antimicrobial studies: Gram-positive (*Bacillus megaterium*) and Gram-negative (*Pseudomonas fluorescens*) bacteria was employed for this study. A volume of 0.1 mL of bacterial cells underwent centrifugation at 8000 rpm for 3 min, followed by a single wash in phosphate-buffered saline. The cells were then re-suspended in nutrient broth. Simultaneously, the PVP-based hydrogels were prepared and cut into discs. These discs were placed into 1 mL of the bacterial suspension, previously mentioned, in 1.5 mL culture tubes and incubated for 24 h. Subsequently, the diluted culture solutions from each test were plated on nutrient agar plates to determine the bacterial counts [36]. After an overnight incubation, the colony forming units (CFU) on the plates were enumerated.

Evaluation of UV blocking performance: To evaluate the UV-blocking properties of PVP-ALG/ZnO nanocomposite film, their effectiveness as sunscreen formulations was tested. The PVP-ALG/ZnO nanocomposite films were blended into pure NIVEA cream at varying concentrations (1-20 wt.%) [25]. The components were thoroughly mixed to ensure the creams were uniform.

In vitro SPF (sun protection factor) was determined using a method described in earlier research [37]. The UV-blocking efficiency of the PVP-ALG and PVP-ALG/ZnO nanocomposite samples was assessed by measuring their UV transmittance at concentrations of 5%, 10%, 15% and 20%. The sunscreen formulations were prepared by combining each sample with cream in the specified concentrations. A UV-Vis spectrophotometer was used to measure the UV transmittance in the wavelength range of 290-400 nm. The obtained transmittance data were used to calculate the SPF values using the formula provided in previous studies [37].

$$\text{SPF} = \sum_{290}^{400} \frac{\sum E_\lambda S_\lambda}{\sum E_\lambda S_\lambda T_\lambda}$$

here, E_λ represents the erythema action spectrum defined by the CIE (Commission Internationale de l'Éclairage) in 1989; S_λ refers to the solar spectrum [38]; while T_λ corresponds to the transmission spectrum of each sample as measured.

RESULTS AND DISCUSSION

Preparation of hydrogel nanocomposite: The synthesis of PVP-ALG/ZnO hydrogel nanocomposites was conducted according to the procedures outlined in the experimental section. In Fig. 1a, visual representations of the pure hydrogel and, in Fig. 1b, the hydrogel nanocomposite are presented. It

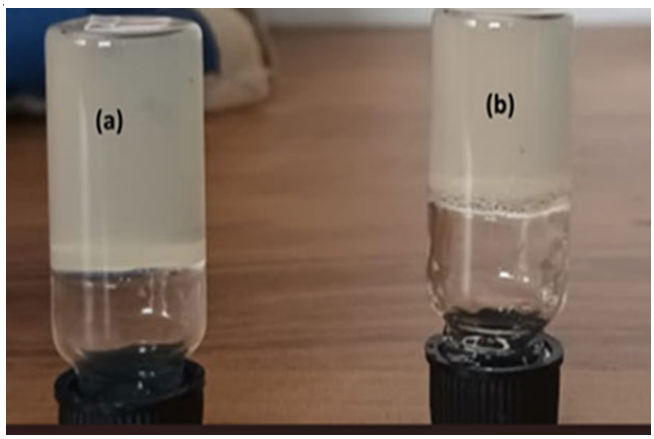

Fig. 1. Image of (a) pure hydrogel (b) hydrogel nanocomposite

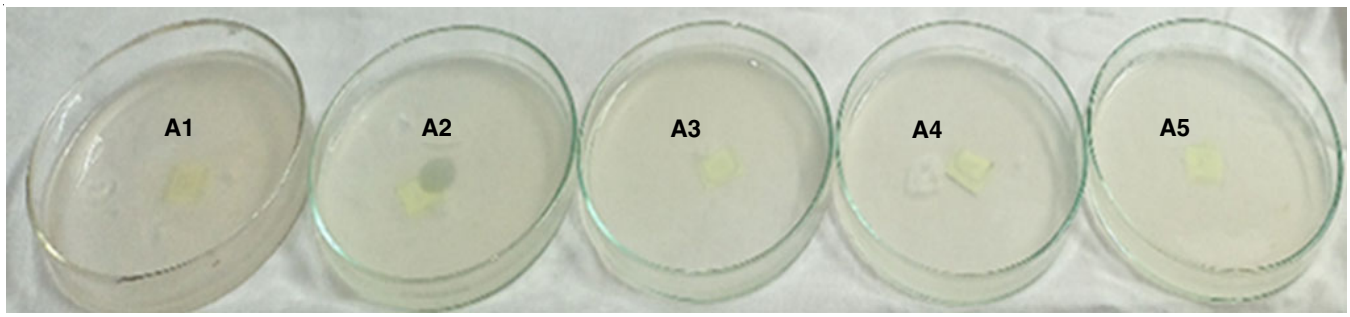

Fig. 2. Images of PVP-ALG/ZnO nanocomposite at different ZnO concentrations

is evident from the images that the incorporation of ZnO nanoparticles does not alter the overall consistency of the hydrogel. Fig. 2, illustrates the hydrogel nanocomposite film, providing further insight into the composite structure and morphology.

The X-ray diffraction (XRD) patterns depicted in Fig. 3 reveal well-defined and intense diffraction peaks, indicative of the high crystallinity of ZnO nanocrystals. No discernible peaks attributed to impurities were observed. The specific 2θ values corresponding to the diffraction peaks at 31.75º, 34.44º, 36.27º, 47.53º, 56.61º, 62.87º, 66.35º, 67.96º, 69.09º, are associated with (100), (002), (101), (102), (110), (103), (200), (112) and (201) planes, these values align closely with the standard reference cards for ZnO (JCPDS file No: 79-2205), confirming the crystallographic nature of the nanoparticles and are indicated in Table-3. The sharpness and intensity of the peaks further highlight the highly crystalline quality of the ZnO nanocrystals. The average crystallite size of the sample (D) was determined using Debye-Scherrer's equation:

$$D = \frac{0.9\lambda}{\beta \cos\theta}$$

where λ represents the wavelength of X-ray radiation; θ denotes the diffraction angle and β corresponds to the full width at half maximum (FWHM) intensity. The determined average crystallite size is 35.687 nm.

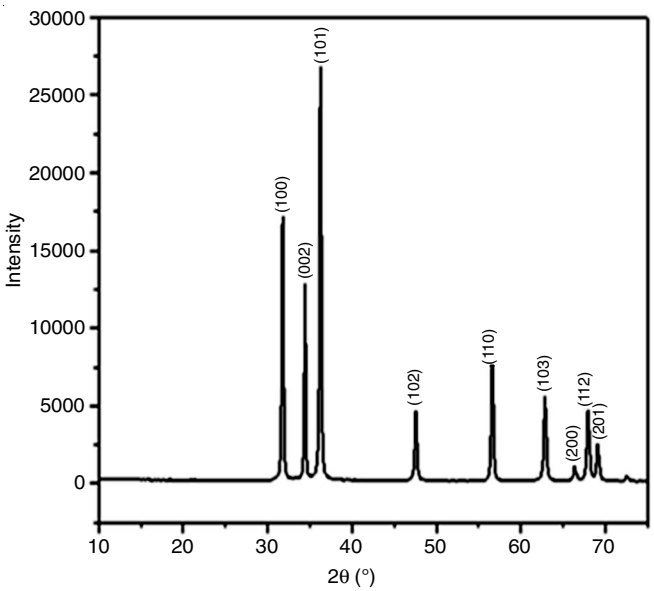

Fig. 3. XRD pattern of ZnO nanoparticle

TABLE-3
THE OBSERVED AND STANDARD 2θ VALUES OF XRD DATA OF ZINC OXIDE NANOPARTICLES

Observed 2θ	Standard 2θ	*h k l*
31.75	31.76	100
34.44	34.41	002
36.27	36.25	101
47.53	47.53	102
56.61	56.59	110
62.87	62.85	103
66.35	66.37	200
67.96	67.94	112
69.00	69.08	201

Morphology studies: The SEM image (Fig. 4a) shows the uniform distribution and compact arrangement of ZnO nanocrystals, exhibiting a distinctive rod-like structure. Whereas, Fig. 4b presents the transmission electron microscopy (TEM) image, further validates that the ZnO particles have developed into a rod-like shape, with a length of about 650 nm and a diameter ranging from 90 to 125 nm and demonstrates their good uniformity. Fig. 5a-b, depicts the FE-SEM images of the dried PVP-ALG hydrogel and PVP-ALG/ZnO nanocomposite. Addition of ZnO nanoparticle showed the white spots on the surface of hydrogel nanocomposite. The tendency of clustering of nanoparticle is visible as the white spots in FE-SEM image are non-uniform.

FTIR studies: Fig. 6 illustrates the FTIR spectra for PVP-ALG hydrogel film, PVP-ALG/ZnO nanocomposite, alginate and PVP powder. The PVP spectra exhibit a distinctive absorption band at 1645 cm^{-1} for carbonyl stretching vibration (C=O) and 1290 cm^{-1} is for the stretching vibration of C-N group. The alginate displayed a wide band at 3290 cm^{-1} related to O-H stretching. Sharp band at 1586 cm^{-1} is attributed to -COO^- asymmetric stretching vibration, while the band at 1410 cm^{-1} is associated with -COO^- symmetric stretching vibration. The C-O stretching peaks were observed at 1023 cm^{-1}. The characteristic peaks of the PVP-ALG blended film are displaced compared to those of the original PVP and alginate. This indicates that molecular interactions and compatibility exist among the polymer chains of PVP and alginate. In comparison to pure PVP-ALG hydrogel film, PVP-ALG/ZnO nanocomposite films exhibited a similar pattern without any significant shift in peak positions. This suggests that there was no significant chemical interaction at the interface between the PVP-ALG matrix and ZnO, which restricted the enhancement of their thermal and barrier properties [39,40].

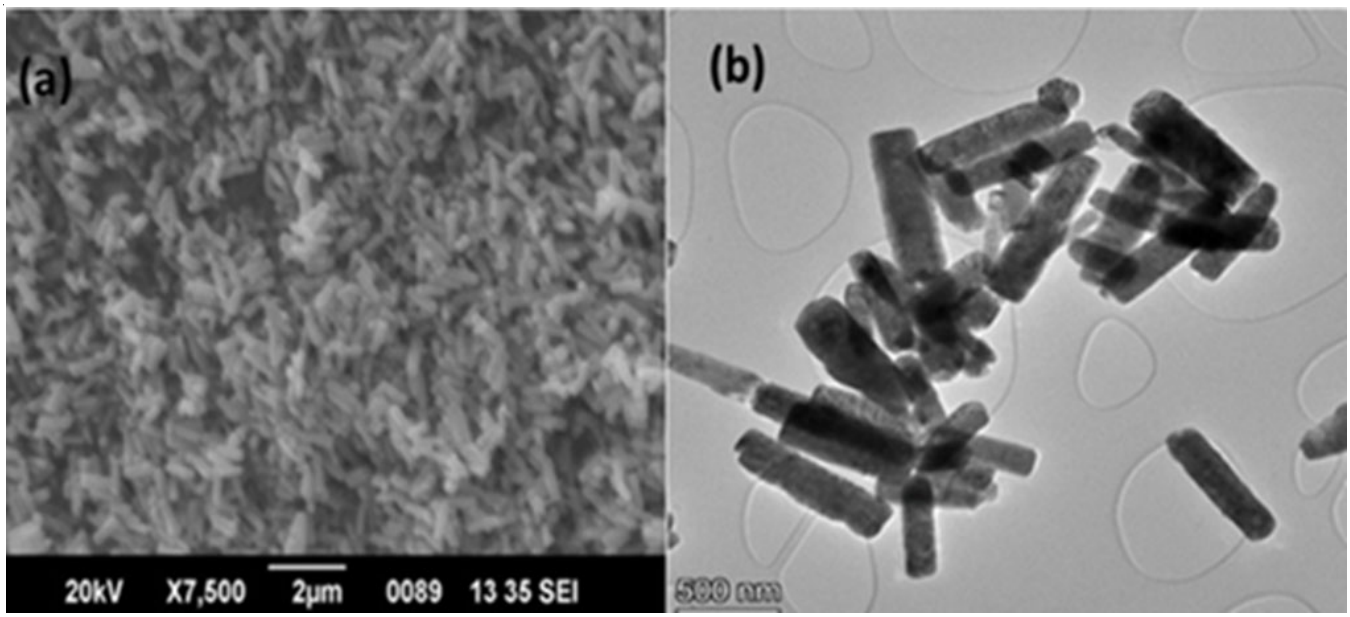

Fig. 4. (a) SEM image of ZnO nanoparticle (b) TEM image of ZnO nanoparticle

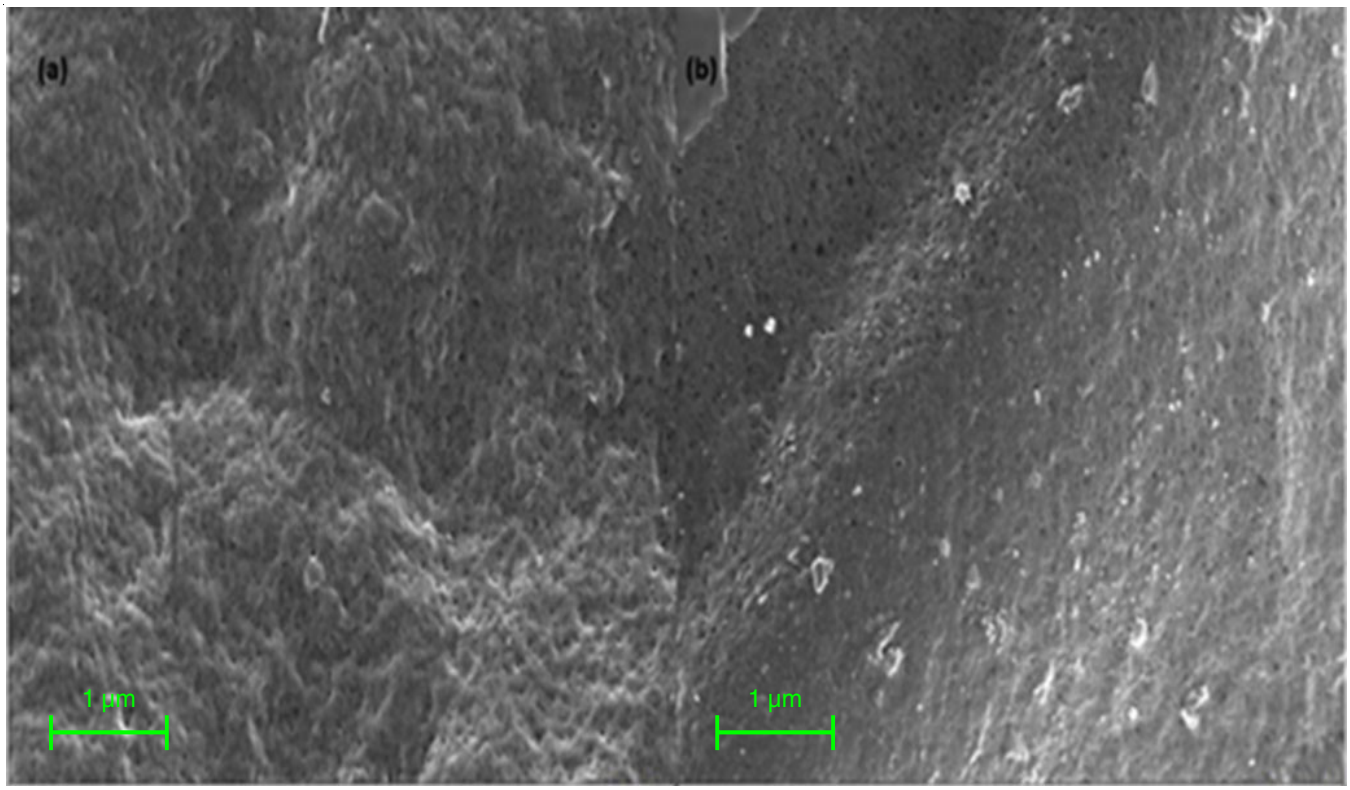

Fig. 5. FE-SEM image of (a) PVP-ALG hydrogel (b) PVP-ALG/ZnO nanocomposite

Mechanical properties: Tensile strength analysis of PVP/alginate hydrogel films are given in Table-4, whereas the graphical representation is shown in Fig. 7. The results shows that the PVP/Alginate ratio 10:90 has high tensile strength and selected for the preparation of hydrogel nanocomposite. Table-5 gives the tensile strength studies of PVP/Alginate hydrogel nanocomposite containing different amounts of ZnO nanoparticle and the graphical representation is illustrated in Fig. 8. The maximum tensile strength value is observed for composite containing 0.0075 g concentration of ZnO and then its value decreases with increase in ZnO concentration. The initial rise in tensile strength can be attributed to the effective dispersion of ZnO particles throughout the polymeric matrix. In this case, ZnO particles act as reinforcement for PVP-ALG-based films. However, the reduction in tensile strength observed beyond a concentration of 0.0075 g is likely due to the clustering of ZnO nanoparticles [29,32]. Henceforth, the PVP-ALG-Z1 composition is chosen for subsequent investigations, given that

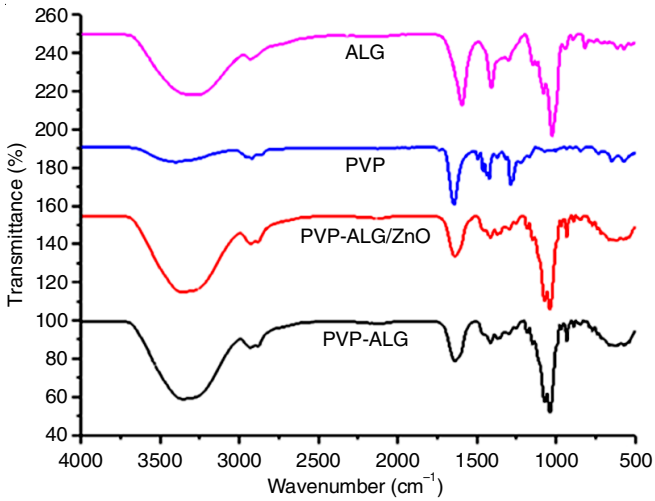

Fig. 6. FTIR spectra of PVP-ALG, PVP-ALG/ZnO, PVP and ALG

TABLE-4
MECHANICAL PROPERTIES OF PVP-ALG HYDROGELS

Sample index	Tensile strength (Nmm^{-2})
PVP-ALG (10:90)-ALG1	8.1599 ± 0.90
PVP-ALG (20:80)-ALG2	6.4445 ± 0.46
PVP-ALG (50:50)-ALG3	6.0521 ± 0.45
PVP-ALG (80:20)-ALG4	5.9520± 0.14
PVP-ALG (90:10)-ALG5	5.4077± 0.60

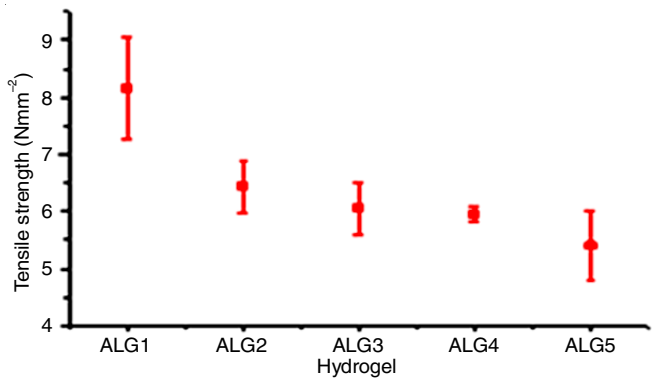

Fig. 7. Mechanical properties of PVP-ALG hydrogels

TABLE-5
MECHANICAL PROPERTIES OF PVP-ALG/ZnO HYDROGEL NANOCOMPOSITE

Sample index	Tensile strength (Nmm^{-2})
PVP-ALG/Z0	8.15922 ± 0.90
PVP-ALG/Z1	11.44090 ± 0.45
PVP-ALG/Z2	8.14660 ± 0.80
PVP-ALG/Z3	7.43680 ± 0.70
PVP-ALG/Z4	6.53790 ± 0.70
PVP-ALG/Z5	5.82377 ± 0.56

the mechanical properties hold significant importance as a condition for biomedical applications.

Swelling studies: The capacity of hydrogels to expand in aqueous environments is a crucial feature for their suitability as wound dressing materials [41]. It has been documented that pH serves as a vital external stimulus influencing the swelling behaviour. Fig. 9 illustrates that the pure hydrogel exhibits a lower degree of swelling compared to the nanocomposite

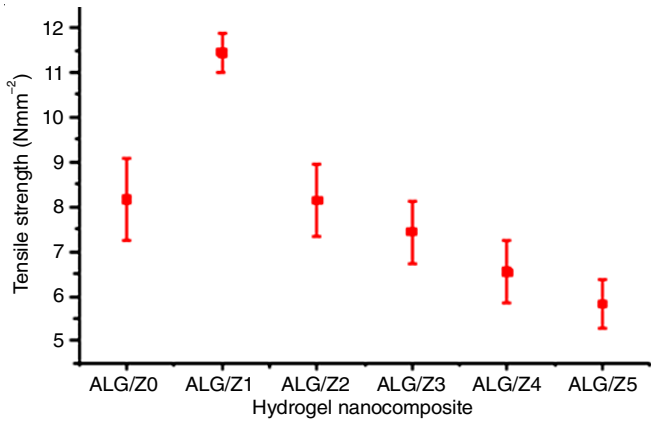

Fig. 8. Mechanical properties of PVP-ALG/ZnO hydrogel nanocomposite

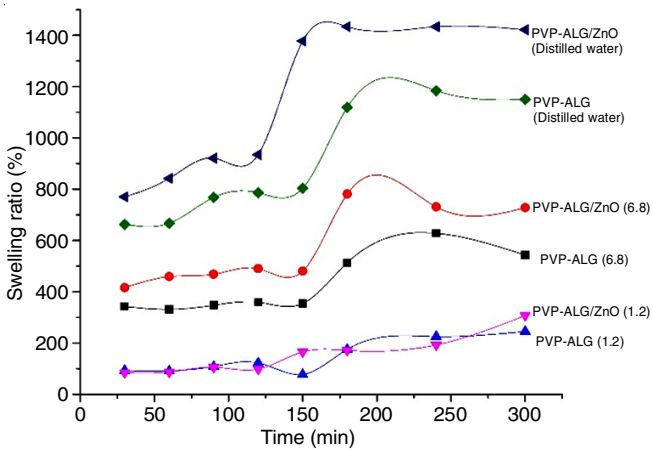

Fig. 9. Percentage swelling with time in distilled water and buffer solution

hydrogels in both distilled water and buffer solution of pH 6.8. The swelling behaviour is similar at pH 1.2. The increased swelling observed in distilled water can be attributed to electrostatic repulsion between ZnO nanoparticles [42]. This repulsion, in turn, expands the crosslinked chains, enlarging hydrogel pores and facilitating the absorption of a greater number of water molecules. The reduction in swelling at acidic pH 1.2 can be ascribed to the protonation of COO^- groups, leading to a tighter crosslinking through hydrogen bonding. Conversely, at higher pH (pH 6.8), the ionization of carboxylic acid groups occurs due to the pK_a of alginate is in the range of 3.4 to 4.4 [43]. Consequently, the hydrogen bonds are disrupted, causing the electrostatic repulsion between macromolecules. This facilitates the easier diffusion of water molecules into the network, resulting in a higher swelling ratio [44].

Drug release studies: Drugs are commonly incorporated into hydrogels through physical encapsulation [45]. Although the hydrogel exhibits a higher swelling capacity in distilled water, drug-loading experiments were performed at pH 6.8 to simulate intestinal fluid, which typically has a pH range of 6 to 7.4. The amounts of cephalexin encapsulated in the PVP-ALG hydrogel and the PVP-ALG/ZnO nanocomposite hydrogel were found to be 16.02 % and 28.16%, respectively. The PVP-ALG/ZnO nanocomposite demonstrated a greater loading capacity for cephalexin, which is ascribed to its superior swelling ability compared to the pure hydrogel.

The drug release profiles of the two samples over time are presented graphically in Fig. 10. As seen, the amount of cephalexin released from the PVP-ALG/ZnO nanocomposite is lower than that from the PVP-ALG hydrogel. This reduction in drug release may result from the interaction between the dispersed ZnO particles and the drug within the hydrogel matrix at pH 6.8, which hinders drug release. Moreover, the gradual dissolution of ZnO nanoparticles might contribute to the sustained release of cephalexin from the nanocomposite [46]. These results indicate that the PVP-ALG/ZnO nanocomposite demonstrates a decreased drug release rate under acidic conditions (pH 6.8) while exhibiting the potential for the controlled and sustained delivery of cephalexin.

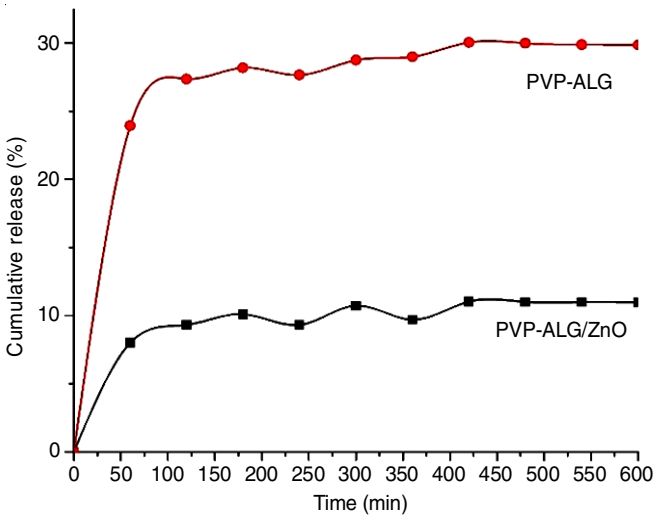

Fig. 10. Release profile of cephalexin from hydrogel and hydrogel composite

Antibacterial assay: The investigation of antimicrobial properties in hydrogel films holds significant importance for their potential applications in the biomedical field. Fig. 11a-b depict the antibacterial impact of hydrogels on *B. megaterium* and *P. fluorescens*, as evidenced by the quantification of colony formation. The results shows that the hydrogel nanocomposite containing ZnO nanoparticles exhibit more antibacterial activity than blank hydrogel. The control, pure PVP-ALG hydrogel and PVP-ALG/ZnO nanocomposite exhibited relative bacterial colony numbers of 730 × 10^6, 90 × 10^6 and 0 CFU for *B. megaterium* and 640 × 10^6, 230 × 10^6 and 160 × 10^6 CFU for *P. fluorescens*, respectively, on the nutrient agar plates. While comparing the antibacterial inhibition of PVP-ALG/ZnO nanocomposite against the two studied strains of bacteria, it is observed that PVP-ALG/ZnO nanocomposite film is more antibacterial towards *B. megaterium.* This lower antimicrobial inhibition of *P. fluorescens* is due to the intrinsic and acquired resistance of *Pseudomonas* genus to several antimicrobial agent [47].

Assessment of UV-blocking efficiency and sun protection factor in cream-based sunscreen formulations: The sunscreen's ability to protect the skin from UVB radiation is generally represented by its sun protection factor (SPF). SPF is defined as the ratio of the time or energy required to produce erythema or sunburn on skin treated with sunscreen to that required on untreated skin [48]. In this work, the PVP-ALG/ZnO (15%) formulation demonstrated the lowest UV transmittance across all tested concentrations. The UV transmittance analysis indicates that Nivea cream offers moderate protection against UVB radiation (280-320 nm) but limited protection against UVA radiation (320-400 nm). While PVP-ALG and

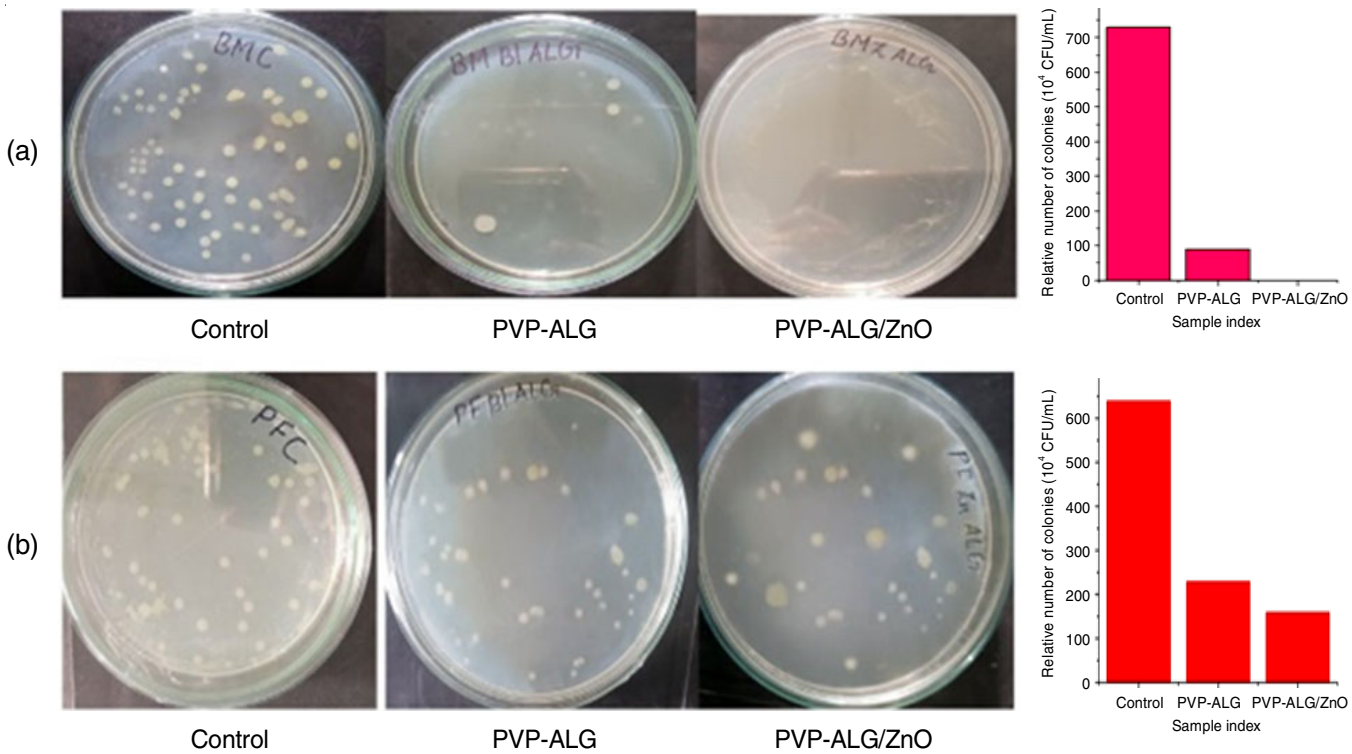

Fig. 11. Photographs of growth of bacterial colonies in PVP-ALG/ZnO nanocomposite (a) *Bacillus megaterium* (b) *Pseudomonas fluorescens*

pure zinc oxide offer some protection against UVA and UVB radiation, the PVP-ALG/ZnO composite, demonstrates superior protection against both UVB and UVA radiation (Fig. 12).

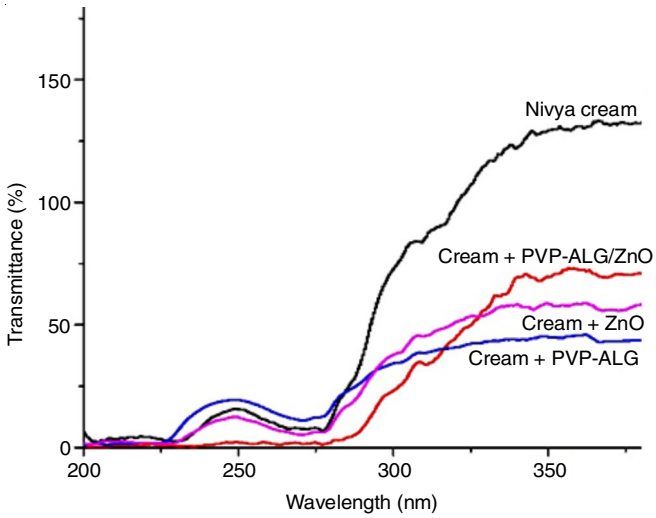

Fig. 12. Transmittance spectra of sunscreen formulations

Furthermore, the transmittance data were used to calculate the sun protection factor (SPF). Nivea cream had an SPF of 2.89, whereas the PVP-ALG hydrogel and PVP-ALG/ZnO nanocomposite formulations had SPFs of 6.5 and 7.9, respectively. Pure ZnO cream formulations, for comparison, had an SPF of 2. Consequently, the formulations incorporating ZnO particles demonstrate substantial promise as an additive in sunscreen suitable for all skin types.

Conclusion

The antibacterial PVP-ALG/ZnO hydrogel nanocomposite film through solution casting method is successfully prepared. The prepared nanocomposites were analyzed using XRD, SEM and TEM techniques. The hydrogel with 0.0075 g ZnO nanoparticle composition were selected for further studies due to its enhanced mechanical property. Swelling studies were carried out in distilled water as well as at an adjusted pH of 6.8, 1.2 and observed that hydrogel nanocomposite shows better swelling ability in pH 6.8 as well as in distilled water compared to pure hydrogel. Both the samples showed almost identical swelling pattern in pH 1.2. The incorporation of ZnO nanoparticles into the PVP-ALG hydrogel slightly enhances the structural integrity and facilitates a more controlled and sustained release of cephalexin. This suggests that the PVP-ALG/ZnO nanocomposite could be a promising candidate for the drug delivery systems requiring prolonged release profiles. The PVP-ALG/ZnO shows greater antibacterial property compared to that of PVP-ALG hydrogel towards *B. megaterium* as well as *P. fluorescens*. The combination of PVP-ALG and ZnO in sunscreen formulations significantly enhances the UV protection, offering superior blocking of both UV radiation compared to individual components or standard formulations like Nivea cream. The PVP-ALG/ZnO composite, with its highest SPF of 7.9, demonstrates strong potential as an effective and versatile sunscreen additive. Based on these findings, the developed PVP-ALG/ZnO nanocomposite hydrogels are promising material for various medical applications including drug delivery, wound healing, *etc*. This innovative approach resulted in the development of advanced nanocomposite PVP-ALG/ZnO film, offering significant potential for transformative applications in bio- and pharmaceutical-based nanotechnology.

CONFLICT OF INTEREST

The authors declare that there is no conflict of interests regarding the publication of this article.

REFERENCES

1. J. Kopeèek and J. Yang, *Polym. Int.*, **56**, 1078 (2007); https://doi.org/10.1002/pi.2253
2. N.A. Peppas, J.Z. Hilt, A. Khademhosseini and R. Langer, *Adv. Mater.*, **18**, 1345 (2006); https://doi.org/10.1002/adma.200501612
3. F. Ganji and M.J. Abdekhodaie, *Carbohydr. Polym.*, **74**, 435 (2008); https://doi.org/10.1016/j.carbpol.2008.03.017
4. C. Wang, R.R. Varshney and D.-A. Wang, *Adv. Drug Deliv. Rev.*, **62**, 699 (2010); https://doi.org/10.1016/j.addr.2010.02.001
5. M. Malini, M. Thirumavalavan, W.-Y. Yang, J.-F. Lee and G. Annadurai, *Int. J. Biol. Macromol.*, **80**, 121 (2015); https://doi.org/10.1016/j.ijbiomac.2015.06.036
6. A.K. Gaharwar, N.A. Peppas and A. Khademhosseini, *Biotechnol. Bioeng.*, **111**, 441 (2014); https://doi.org/10.1002/bit.25160
7. K. Haraguchi, *Curr. Opin. Solid State Mater. Sci.*, **11**, 47 (2007); https://doi.org/10.1016/j.cossms.2008.05.001
8. E. Larrañeta, S. Stewart, M. Ervine, R. Al-Kasasbeh and R. Donnelly, *J. Funct. Biomater.*, **9**, 13 (2018); https://doi.org/10.3390/jfb9010013
9. T.R. Hoare and D.S. Kohane, *Polymer*, **49**, 1993 (2008); https://doi.org/10.1016/j.polymer.2008.01.027
10. N.S. Satarkar, D. Biswal and J.Z. Hilt, *Soft Matter*, **6**, 2364 (2010); https://doi.org/10.1039/b925218p
11. L. Zhao, L. Xu, H. Mitomo and F. Yoshii, *Carbohydr. Polym.*, **64**, 473 (2006); https://doi.org/10.1016/j.carbpol.2005.12.014
12. S. Benamer, M. Mahlous, A. Boukrif, B. Mansouri and S.L. Youcef, *Nucl. Instrum. Methods Phys. Res. B*, **248**, 284 (2006); https://doi.org/10.1016/j.nimb.2006.04.072
13. A. Zheng, Y. Xue, D. Wei, S. Li, H. Xiao and Y. Guan, *Soft Mater*, **12**, 179 (2014); https://doi.org/10.1080/1539445X.2013.831357
14. N. Roy, N. Saha, T. Kitano and P. Saha, *J. Appl. Polym. Sci.*, **117**, 1703 (2010); https://doi.org/10.1002/app.32056
15. N. Roy, N. Saha, T. Kitano and P. Saha, *J. Appl. Polym. Sci.*, **117**, 1703 (2010); https://doi.org/10.1002/app.32056
16. M. Wang, L. Xu, H. Hu, M. Zhai, J. Peng, Y. Nho, J. Li and G. Wei, *Nucl. Instrum. Methods Phys. Res. B*, **265**, 385 (2007); https://doi.org/10.1016/j.nimb.2007.09.009
17. M. Risbud, A. Hardikar and R. Bhonde, *J. Biosci.*, **25**, 25 (2000); https://doi.org/10.1007/BF02985178
18. N. Isiklan, M. Inal and M. Yigitoglu, *J. Appl. Polym. Sci.*, **110**, 481 (2008); https://doi.org/10.1002/app.28577
19. K.Y. Lee and D.J. Mooney, *Prog. Polym. Sci.*, **37**, 106 (2012); https://doi.org/10.1016/j.progpolymsci.2011.06.003
20. W.R. Gombotz and S.F. Wee, *Adv. Drug Deliv. Rev.*, **31**, 267 (1998); https://doi.org/10.1016/S0169-409X(97)00124-5
21. A. Agarwal, J.F. McAnulty, M.J. Schurr, C.J. Murphy and N.L. Abbott, Polymeric Materials for Chronic Wound and Burn Dressings In: Advanced Wound Repair Therapies, Woodhead Publishing Series in Biomaterials, Chap. 8 pp. 186–208 (2011).

22. S.Y. Nam, Y.C. Nho, S.H. Hong, G.T. Chae, H.S. Jang, T.S. Suh, W.S. Ahn, K.E. Ryu and H.J. Chun, *Macromol. Res.*, **12**, 219 (2004); https://doi.org/10.1007/BF03218391
23. P.J.P. Espitia, N.D.F.F. Soares, J.S.D.R. Coimbra, N.J. De Andrade, R.S. Cruz and E.A.A. Medeiros, *Food Bioprocess Technol.*, **5**, 1447 (2012); https://doi.org/10.1007/s11947-012-0797-6
24. R. Kumar, A. Umar, G. Kumar and H.S. Nalwa, *Ceram. Int.*, **43**, 3940 (2017); https://doi.org/10.1016/j.ceramint.2016.12.062
25. D. Kai, Y.K. Chua, L. Jiang, C. Owh, S.Y. Chan and X.J. Loh, *RSC Adv.*, **6**, 86420 (2016); https://doi.org/10.1039/C6RA21433A
26. C. Hanley, J. Layne, A. Punnoose, K.M. Reddy, I. Coombs, A. Coombs, K. Feris and D. Wingett, *Nanotechnology*, **19**, 295103 (2008); https://doi.org/10.1088/0957-4484/19/29/295103
27. A.K. Barui, R. Kotcherlakota and C.R. Patra, Biomedical Applications of Zinc Oxide Nanoparticles, In: Inorganic Frameworks as Smart Nanomedicines, Wiliam Andrew Applied Science Publishers: New York, Chap. 6, pp. 239–278 (2018).
28. N. Serpone, D. Dondi and A. Albini, *Inorg. Chim. Acta*, **360**, 794 (2007); https://doi.org/10.1016/j.ica.2005.12.057
29. J. Markus, R. Mathiyalagan, Y.-J. Kim, Y. Han, Z.E. Jiménez-Pérez, S. Veronika and D.-C. Yang, *New J. Chem.*, **43**, 9188 (2019); https://doi.org/10.1039/C8NJ06044D
30. F. Feng, C. Hao, H. Zhang, W. Xie, X. Wang and Y. Zhao, *J. Mater. Sci. Mater. Electron.*, **26**, 6704 (2015); https://doi.org/10.1007/s10854-015-3273-z
31. Y.K. Su, S.M. Peng, L.W. Ji, C.Z. Wu, W.B. Cheng and C.H. Liu, *Langmuir*, **26**, 603 (2010); https://doi.org/10.1021/la902171j
32. M. Entezam, H. Daneshian, N. Nasirizadeh, H.A. Khonakdar and S.H. Jafari, *Macromol. Mater. Eng.*, **302**, 1600397 (2017); https://doi.org/10.1002/mame.201600397
33. S. Thambidurai, P. Gowthaman, M. Venkatachalam and S. Suresh, *J. Alloys Compd.*, **830**, 154642 (2020); https://doi.org/10.1016/j.jallcom.2020.154642
34. A. Bakravi, Y. Ahamadian, H. Hashemi and H. Namazi, *Adv. Polym. Technol.*, **37**, 2625 (2018); https://doi.org/10.1002/adv.21938
35. S. Javanbakht and H. Namazi, *Mater. Sci. Eng. C*, **87**, 50 (2018); https://doi.org/10.1016/j.msec.2018.02.010
36. R. Mourad, F. Helaly, O. Darwesh and S.E. Sawy, *Cont. Lens Anterior Eye*, **42**, 325 (2019); https://doi.org/10.1016/j.clae.2019.02.007
37. R. Kaur, N.S. Thakur, S. Chandna and J. Bhaumik, *J. Mater. Chem. B Mater. Biol. Med.*, **8**, 260 (2020); https://doi.org/10.1039/C9TB01569H
38. D.A.J. Connolly and A.R. Wilcox, *J. Sports Med. Phys. Fitness*, **40**, 35 (2000).
39. D. Kim, Y. Lee, J. Seo, H. Han and S.B. Khan, *Polym. Int.*, **62**, 257 (2013); https://doi.org/10.1002/pi.4294
40. J. Seo, G. Jeon, E.U.S. Jang, S. Bahadar Khan and H. Han, *J. Appl. Polym. Sci.*, **122**, 1101 (2011); https://doi.org/10.1002/app.34248
41. C. Wang, M. Wang, T. Xu, X. Zhang, C. Lin, W. Gao, H. Xu, B. Lei and C. Mao, *Theranostics*, **9**, 65 (2019); https://doi.org/10.7150/thno.29766
42. M. Helminger, B. Wu, T. Kollmann, D. Benke, D. Schwahn, V. Pipich, D. Faivre, D. Zahn and H. Cölfen, *Adv. Funct. Mater.*, **24**, 3187 (2014); https://doi.org/10.1002/adfm.201303547
43. M. Nagarsenker and U. Shinde, *Indian J. Pharm. Sci.*, **71**, 313 (2009); https://doi.org/10.4103/0250-474X.56033
44. Y. Yang, X. Wang, F. Yang, L. Wang and D. Wu, *Adv. Mater.*, **30**, 1707071 (2018); https://doi.org/10.1002/adma.201707071
45. Y. Murali Mohan, P.S. Keshava Murthy and K. Mohana Raju, *React. Funct. Polym.*, **63**, 11 (2005); https://doi.org/10.1016/j.reactfunctpolym.2005.01.005
46. D.M. Rata, A.N. Cadinoiu, O.M. Daraba, L.M. Gradinaru, L.I. Atanase and D.L. Ichim, *Pharmaceutics*, **15**, 2240 (2023); https://doi.org/10.3390/pharmaceutics15092240
47. M.P. Silverio, G.B. Kraychete, A.S. Rosado and R.R. Bonelli, *Antibiotics*, **11**, 985 (2022); https://doi.org/10.3390/antibiotics11080985
48. J.A. Ankrum, O.R. Miranda, K.S. Ng, D. Sarkar, C. Xu and J.M. Karp, *Nat. Protoc.*, **9**, 233 (2014); https://doi.org/10.1038/nprot.2014.002